Scientific Research Publishing

Materials Sciences and Applications, 2022, 13, 417-432
https://www.scirp.org/journal/msa
ISSN Online: 2153-1188
ISSN Print: 2153-117X

Experimental Evaluation of Ductile Fracture of Sheet Metals under Plane Stress States

Jian Fang[1*], Bin Wang[2], Jianwei Zhang[1], Xin Yang[3]

[1]Central Research Institute, Baoshan Iron & Steel Co., Ltd., Shanghai, China
[2]Lishi Instruments (Shanghai) Co., Ltd., Shanghai, China
[3]DOM 3D Ltd., Shanghai, China
Email: *fangjian@baosteel.com

How to cite this paper: Fang, J., Wang, B., Zhang, J.W. and Yang, X. (2022) Experimental Evaluation of Ductile Fracture of Sheet Metals under Plane Stress States. *Materials Sciences and Applications*, **13**, 417-432.
https://doi.org/10.4236/msa.2022.136024

Received: May 27, 2022
Accepted: June 26, 2022
Published: June 29, 2022

Abstract

With the application of lightweight materials such as advanced high-strength steel and aluminum alloy in the automotive industry, it is necessary to quantitatively evaluate the ultimate deformation capacity of materials under various plane stress states for the digital simulation of these materials. Conventional Nakajima test can only provide three regular plane stress states, such as tension, plane strain tension and bulging, and FLC curve is affected by deformation path, mold lubrication and other variables. More importantly, Nakajima test cannot provide shear, tension shear, which are extremely important loading conditions in automobile collisions. Therefore, the research work of this paper focuses on the evaluation of the ultimate ductile fracture behavior of sheet metals under various conditions of plane stress states. The four variables Mohr-Coulomb model was established to study the ductile fracture of metal sheets under plane stress states. Beginning with the recorded minor and major strain distributing on the deformation area of uniaxial tension samples, Moving Regression Algorithm was deployed to reveal the inherent relationship among the key parameters involved in the M-C model, which also provided an experimental technique for monitoring the instantaneous changing of triaxiality over the whole loading period. Three or four typical types of uniaxial-loading specimens were well designed to determine the M-C curve. As a result, M-C curve and the transformed major stain vs. minor strain curve provide further information about the material arrest to the ductile fracture in the area of shear loading, in comparison with the conventional FLD test.

Keywords

Digital Image Correlation (DIC), Plane Stress State, Stress Triaxiality, Ductile Fracture

1. Introduction

In order to meet the demand for the safe and lightweight design of passenger cars, Advanced High Strength Steel (AHSS) sheets have become the preferred materials for car body and some passive safety components. Compared with the cold rolled sheets for stamping and conventional high-strength low-alloy steels (HSLA), AHSS is not only excellent in the combination of strength and plastic, but also is more remarkable in local deformability as the result of their unique strengthening mechanism, like phase transformation, twinning and complex phase composition. Therefore, a series of state-of-the-art forming processes such as hydraulic forming, bending, rolling, torsion and hot stamping have further expanded the industrial applications of AHSS. Meanwhile, some structural components in passenger cars endure complex loading states during driving and especially under collision, more attention needs to be paid to the material constitutive relation, the material response, especially the resistance to the ductile fracture under different stress states such as compression, shear, and uniaxial/biaxial tension, necessitated by materials R&D and industrial applications.

On the other hand, Nakajima's Forming Limit Diagram (FLD) test reveals that the arrest performance of sheet metal to the ductile fracture is significantly affected by plane stress loading conditions. As a result, Forming Limit Curve (FLC) defines the material ultimate deformation with respect to the different deformation paths. Through FLD test, Bai and Wierzbicki [1] proposed their analytical criterion models for predicting the stamping failure based on the plane stress triaxiality. However, until now it has still been of a hard job to plot a reproducible and analytical FLC curve through scattering major/minor strain points. Moreover, conventional Nakajima test can only provide three regular plane stress states, like tension, plane strain tension and bulging, and consequent FLC curve is significantly affected by the non-proportional deformation path, mold lubrication and other variables. More importantly, Nakajima test cannot provide shear, tension shear, which are extremely important loading conditions in automobile collision, especially for the components or structures made of light-weight high-strength materials.

Meanwhile, the Generalized Incremental Stress State Dependent Damage Model (GISSMO) in LS-DYNA® is capable to predict the ultimate fracture behavior of the calibrated material in complex strain paths. For new materials, GISSMO needs real-tested tensile force-displacement curves of 5 - 8 types of samples with well-designed geometries, and their DIC frames during all loading periods until fracture to validate and calibrate the material parameters used in the model [2]. However, it was reported that the stress triaxiality confined in the fracture zone varies significantly, due to the loading alignment and the material local deformation [3] [4]. When using the theoretical geometry-related stress triaxiality (η) as the input to GISSMO, inestimable system deviation will be introduced.

Many studies [5] [6] have designed samples with typical theoretical triaxiality and obtained the force-displacement curve of the fracture zone through DIC technology to calibrate the accuracy of Finite Element Method. Then the whole

process of loading the samples to fracture could be simulated to track the evolution history of physical characteristic parameters characterizing the toughness fracture, such as stress triaxiality, Lode angle, equivalent effect strain, etc. Because of the drastic changes, the strain integral averaging method was usually used to determine these characteristic parameters.

In this paper, the inconvenience of the application of FEM in industrial laboratory was avoided instead Moving Regression Algorithm was deployed upon the measured (ε_1, ε_2) to monitor the inherent relationship among the key parameters involved in the four variables Mohr-Coulomb model. That is, the transformation from the originally measured (ε_1, ε_2) into the explicit (η, $\bar{\varepsilon}$) required by M-C model has been well detailed. Also the locus of Mohr-Coulomb fracture curve with the transformed extended FLC curve inclusive of shear and tension-shear definition was also introduced to characterize the material resistance to the ductile fracture under various plane stress conditions.

2. Theoretical Model

Due to the requirement of thickness reduction and lightweight, AHSS sheets are usually delivered with thin thickness, so the material mainly experiences the plane stress state in service. Similar to the FLC representing various stamping deformation paths, the plane stress plasticity could be expressed by the principle true major strain ε_1 in loading direction and the true minor strain ε_2. Then, the strain ratio α is calculated by Equation (1).

$$\alpha = \Delta\varepsilon_2 / \Delta\varepsilon_1 \tag{1}$$

α in Equation (1) represents the slope of the curve of minor strain (ε_2) against major strain (ε_1) at a certain time. The regular FLD test shall consist of a group of samples, relative to three kinds of strain ratio: $\alpha = -0.5$ is uniaxial tension, $\alpha = 0$ is plane strain tension, and $\alpha = 1$ is equibiaxial bulging. It should be noted that for the ideal specimen with special design, under the proportional loading or proportional strain path, the strain ratio can be simplified as the ratio of $\alpha\varepsilon_2$ to ε_1. However, the stress triaxiality usually changes with the deformation of the specimen under real conditions. Therefore, in the present study, the moving regression algorithm was applied to calculate the linear regression slope of each (ε_1, ε_2) scatter point to obtain the instantaneous α. Where N is the smooth bandwidth, which means N pairs of (ε_1, ε_2) scatter points neighbor to the event of η_i are to be included by using linear regression algorithm to obtain the final result, see Equations (2) and (3). The larger value of N causes the more smooth evolution curve of instantaneous η_i.

$$\eta_i = \frac{\Delta\varepsilon_2}{\Delta\varepsilon_1} \simeq \frac{\sum_{j=i-\frac{N-1}{2}}^{i+\frac{N-1}{2}} \varepsilon_{1,j}\varepsilon_{2,j} - N\bar{\varepsilon}_1\bar{\varepsilon}_2}{\sum_{j=i-\frac{N-1}{2}}^{i+\frac{N-1}{2}} \varepsilon_{1,j}^2 - N\bar{\varepsilon}_1^2} \qquad i = 1,2,3,\cdots,m \tag{2}$$

$$\bar{\varepsilon}_1 = \frac{\sum_{j=i-\frac{N-1}{2}}^{i+\frac{N-1}{2}} \varepsilon_{1,j}}{N}, \quad \bar{\varepsilon}_2 = \frac{\sum_{j=i-\frac{N-1}{2}}^{i+\frac{N-1}{2}} \varepsilon_{2,j}}{N} \qquad i = 1, 2, 3, \cdots, m \tag{3}$$

Since the z-component stress is neglected under the plane stress state, *i.e.* $\sigma_3 = 0$, the point (ε_1, ε_2) in real-tested strain space could be transformed into the point (σ_1, σ_2) as in the stress space [1], then the stress ratio β is as expressed in Equation (4).

$$\beta = \sigma_2 / \sigma_1 = \frac{2\alpha + 1}{2 + \alpha} \tag{4}$$

Introducing the stress triaxiality η and Lode angle parameter $\bar{\theta}$, the (σ_1, σ_2, σ_3) in the Cartesian-coordinate stress space could also be transformed into corresponding points of ($\bar{\sigma}$, η, $\bar{\theta}$) or ($\bar{\varepsilon}$, η, $\bar{\theta}$) in the virtual spherical-coordinate stress or strain space respectively. All the variables can be determined through Equation (5) to Equation (8) [1] [7].

$$\eta = \frac{\sigma_m}{\bar{\sigma}} = \frac{\beta + 1}{3\sqrt{\beta^2 - \beta + 1}} \tag{5}$$

$$\bar{\theta} = 1 - \frac{2}{\pi} \arccos \xi \tag{6}$$

$$\xi = -\frac{27}{2} \eta \left(\eta^2 - \frac{1}{3} \right) \tag{7}$$

$$\mathrm{d}\bar{\varepsilon} = \frac{2\mathrm{d}\varepsilon_1}{\sqrt{3}} \sqrt{1 + \alpha + \alpha^2} \tag{8}$$

Under the proportional loading of plane stress condition, the strain ratio α is constant, so that Equation (8) can be integrated and transformed into the Equation (9).

$$\bar{\varepsilon} = \frac{2\varepsilon_1}{\sqrt{3}} \sqrt{1 + \alpha + \alpha^2} \tag{9}$$

It should be noted that $\bar{\sigma}$ and $\bar{\varepsilon}$ are equivalent true stress and strain respectively in the spherical-coordinate space. So far, if the plane stress is applied to the specimen, the corresponding local plane stress triaxiality η, Lode angle parameter $\bar{\theta}$ and equivalent true strain $\bar{\varepsilon}$ can be simultaneously calculated through the recorded major and minor true strains (ε_1, ε_2) on the local area of interest over all the loading duration. As a result, the characteristic value of $\bar{\varepsilon}_f$ affected by the change of η implies the resistance performance of sheet metals to the ductile fracture, as experimentally studied in the paper.

On the other hand, Mohr Coulomb fracture model establishes the analytical relationship between loading triaxiality η and equivalent strain $\bar{\varepsilon}$, which has been widely confirmed [7] [8] [9] [10]. Without considering anisotropy, the four-variable M-C model was described as Equation (11), here Hollomon flow hardening rule was included for simplification, see Equation (10):

$$\bar{\sigma} = K\bar{\varepsilon}^{n} \tag{10}$$

K is the strain strengthening coefficient obtained by the uniaxial tensile test (unit: MPa) and n is the strain hardening exponent.

$$\frac{c_2}{\sqrt{\frac{1+c_1^2}{3}}\cos\left(\frac{\bar{\theta}\pi}{6}\right)+c_1\left[\eta+\frac{1}{3}\sin\left(\frac{\bar{\theta}\pi}{6}\right)\right]} = \left\{c_\theta^s+\left(c_\theta^{ax}-c_\theta^s\right)\cdot\frac{\sqrt{3}}{2-\sqrt{3}}\left[\sec\left(\frac{\bar{\theta}\pi}{6}\right)-1\right]\right\}\cdot K\bar{\varepsilon}_{\mathrm{f}}^{n}$$

$$c_\theta^{ax} = \begin{cases} 1 & \bar{\theta} \geq 0 \\ c_\theta^c & \bar{\theta} < 0 \end{cases} \tag{11}$$

Here, $C_1 \geq 0$ and $C_2 > 0$ are both material constants, in which C_1 is dimensionless and C_2 represents the stress (unit: MPa). According to different yield criteria, c_θ^s has different values. For example, when considering von Mises yield condition, $c_\theta^s = 1$, while $c_\theta^s = \sqrt{3}/2$ is Tresca yield condition. Here for sheet samples loaded by uniaxial tension under plane stress states, $c_\theta^c = c_\theta^s = 1$ can be considered as a special case in general.

At present, the GISSMO model in LS-DYNA® has been successfully used to optimize the cold forming process for AHSS and simulate the crashworthiness of passenger cars. As to validate new material parameters required by the GISSMO model through inverse identification procedure, a series of typical uniaxial-tension specimens with their theoretically given stress triaxiality η are well prepared and tested to obtain the load-displacement curve, including the pure shear, shear tension, uniaxial tension, plane strain tension and bulge [4] [11]. Since K, n, η and $\bar{\theta}$ in Equation (11) all can be determined in advance, and the ultimate equivalent true strain $\bar{\varepsilon}_{\mathrm{f}}$ of the fracture zone can be measured by DIC during loading. In principle, it seems that only three or four samples are needed to obtain the four variables in Equation (11), as C_1, C_2, c_θ^s and c_θ^c, through the fitting optimization algorithm. However, the η value fluctuates significantly with the deformation [2] [3] [4], at the same time, η is strongly correlated with $\bar{\theta}$ due to the plane stress state, indicated by Equation (6) and (7). Therefore, different sample types have great influences on the final curve-fitted parameters involved in the M-C model. To simplify the Equation (11), Coefficients a and b were defined as follows.

$$a = \frac{1}{\sqrt{3}}\cos\left(\frac{\bar{\theta}\pi}{6}\right) \tag{9}$$

$$b = \eta + \frac{1}{3}\sin\left(\frac{\bar{\theta}\pi}{6}\right) \tag{10}$$

Under plane stress loading conditions, the coefficients a and b can be solely determined by the given stress triaxiality η as shown in **Figure 1**. The curve of the strain ratio α against η was also plotted in the figure to indicate the characteristic deformation path relative to the current η. All the values under typical

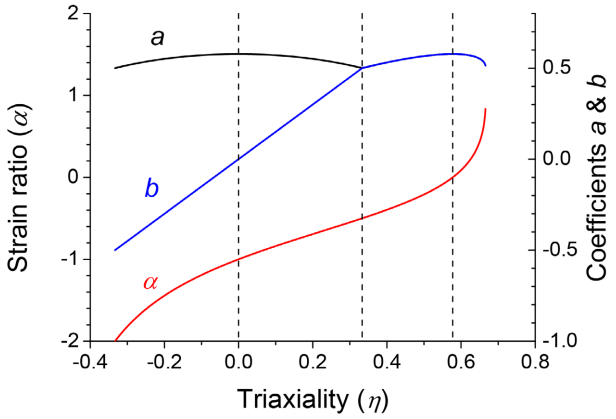

Figure 1. The relationship between coefficients *a*, *b* and *η*, and the relative value of *α*.

Table 1. Parameters for typical plane stress states.

State parameters	Pure shear	Uniaxial tension	Plane strain	Biaxial bulge
Strain ratio α	−1	−0.5	0	1
Triaxiality η	0	$\frac{1}{3}$	$\frac{1}{\sqrt{3}}$	$\frac{2}{3}$
Lode angle parameter $\overline{\theta}$	0	1	0	−1

loading conditions were listed in Table 1.

As shown in Figure 1, when the plane stress triaxiality starts from the uniaxial tension, the coefficients *a* and *b* of the M-C model tend to be the same, covering the regular deep drawing strain paths according to the FLD test, like uniaxial tension, plane strain tension and bulge. Therefore, if choosing these three types of specimen, key parameters linked to the M-C model could hardly be well fitted, no matter how many specimens were involved in the testing.

In the meanwhile, the coefficients *a* and *b* are significantly different in the pure shear and shear-tension regions. As proposed in the present study, Therefore, the research shows that among the three or four samples, at least one pure shear or shear-tension sample, together with a uniformly deformed uniaxial tensile sample are required, in order to accurately fit and optimize the four variable parameters of M-C model, as to accurately predict the ultimate deformation performance of AHSS steel plate under different plane stress loading conditions.

Here in the present study, the approach to establish the M-C model was validated by comparing the reported results of 7075-T6 aluminum sheet in Lee's research on its cold forming performance through GISSMO tools [8].

3. Experimental

LE5105 electro-mechanical testing machine was used to record the tension force-displacement curve, simultaneously the evolution of strain on the specimen local area of interest was simultaneously recorded by 3D-DIC technology (GOM ARAMIS 5M). In general, a regular video extensometer could also be im-

plemented to record the deformation of specimens during loading until breaking for further strain analyzing, illustrated in Figure 2. To meet the GISSMO requirements [2] [12] and concern the importance of the shear specimen mentioned above, at least three types of uniaxial loading specimens including 0˚pure shear (Figure 3(a)), 45˚shear-tension (Figure 3(b)), regular tensile (Figure 3(c)) were recommended in the present study.

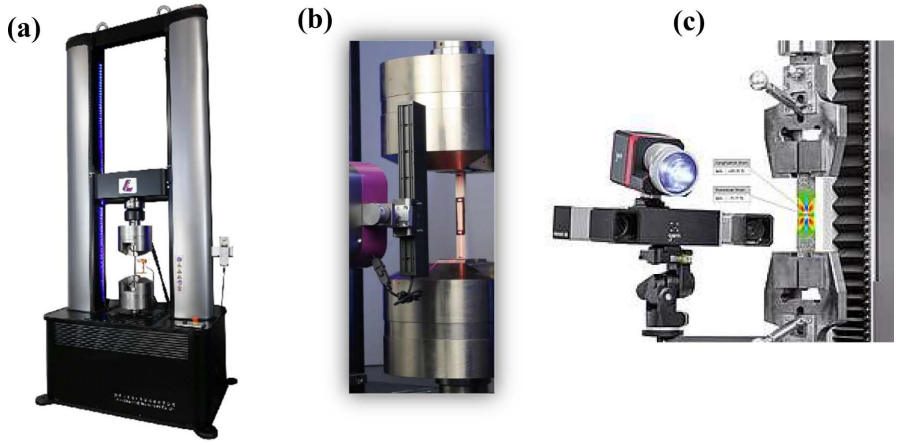

Figure 2. Uniaxial loading tensile machine equipped with DIC analysis devices. (a) Tensile testing machine, (b) 2D-DIC video extensometer, (c) 3D-DIC device.

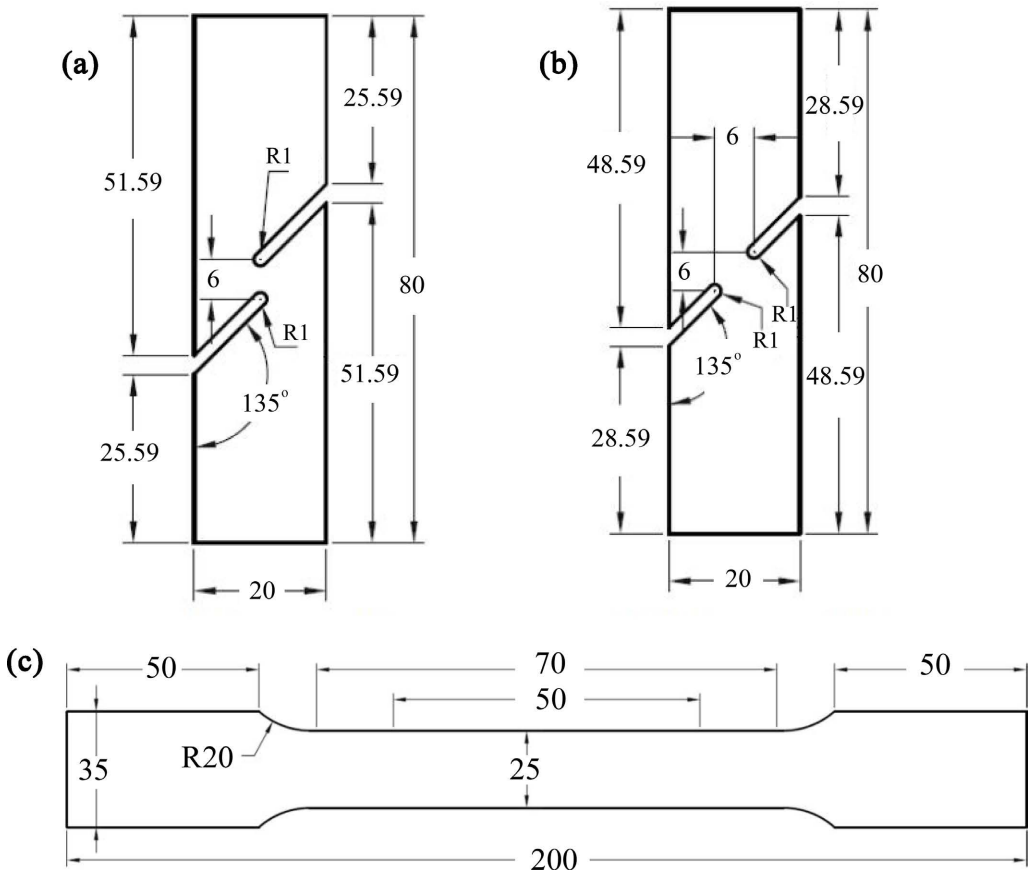

Figure 3. Three types of uniaxial loading specimens used to determine the M-C curve.

It should be addressed that the alignment of the load chain and the centering of the specimen installment could be ensured by the help of laser level adopted. Therefore, each well designed specimen approximately experienced the deformation in the proportional strain path. See **Figure 4**, for all types of specimens as studied, the recorded true major and minor strain scattering points (ε_1, ε_2) of the breaking area are apparently linear from beginning to critical breaking. It is also shown that the Moving Regression Algorithm mentioned above could be reliable to monitor the instantaneous strain ratio α of the studied region at any given time.

The sampling frequency of GOM ARAMIS is 15 fps. Uniaxial loading is applied on the specimen by control the crosshead separation speed. For pure shear and tension-shear specimens, the total length of deformation area is only 6 mm, while the regular tensile specimen has the parallel length up to 70 mm. So the loading speed should be controlled about 2.5 mm/min for shear and shear-tension specimens and 25mm/min for large regular tensile specimen, *i.e.* about 0.04% - 0.05% change in strain every two frames of images, which is compatible to the best measurement capacity of the strain analyzer with its 0.005% accuracy during measurement.

Similar to the FEM calculation, the results of DIC strain measurement is also affected by the initial size of the virtual grid/gauge. In order to calibrate and regularize material parameters, GISSMO requires two series of fine measurement for small samples, like **Figure 3(a)** and **Figure 3(b)**, prepared with two virtual grid sizes (0.5 mm and 1 mm). However, for such large specimens as **Figure 3(c)**, it requires five series of data based on the virtual grid size including 0.5, 1, 2.5, 5 and 10 nm [2] [4]. In general, the smaller the grid size, the more accurate local deformation could be differentiated in detail, while more time consumption and more complex calculation will be performed. Here in the present study, 0.5 mm grid size was used to precisely locate the fracture zone and monitor the

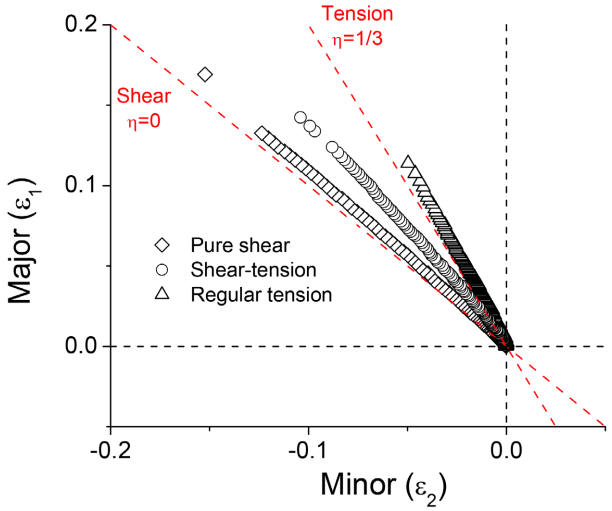

Figure 4. Evolution of major and minor strain on the breaking area of all three types of specimens.

change of the equivalent strain with its relative stress triaxiality as well.

The critical moment of the ductile fracture could be marked as the steep drop on the recorded force-displacement curve in the meanwhile the major and minor strain of the deformation area could be continuously recorded until cracking. Through the last several frame images, the fracture region with the ultimate deformation could be clearly identified. The necessary parameters required by the M-C model could be also evaluated, such as the triaxiality η, the equivalent fracture strain $\bar{\varepsilon}_f$. Repeating for all three types of specimens, key parameters to establish the M-C model, see Equation (11), of the sheet as received, including C_1, C_2, c_θ^s and $c_\theta^c = 1$ (in the present work), could be solely determined, using non-linear curve fitting algorithm.

In this paper, a 1.4 mm-thick, ultra-high-strength and boron-contained steel sheet, 1800UHSS has been studied. The yield strength and the ultimate tensile strength in the rolling direction were 1350 MPa and 1850 MPa respectively, the tensile elongation at fracture was 7%, n value was 0.112, and K value was 2772 MPa. It should be noted that, according to tensile results, the material anisotropy was not very significant (the relative deviation of yield and tensile strength were both less than 5% in three directions 0˚, 45˚ and 90˚), which met the assumption of simplified M-C model.

4. Results and Discussion

4.1. Algorithm Validation in Comparison with the Reported 7075-T6 Aluminum Sheet

The 7075-T6 aluminum sheet can be manufactured into automotive bumper beams by means of cold roll forming process. Lee *et al.* [8] studied the relationship between η and $\bar{\varepsilon}_f$ by using commercial GISSMO tools upon several similar uniaxial loading specimens (see **Figure 5(b)**). The remarkable W-shaped character was reported as the function of $\bar{\varepsilon}_f$ against η, revealed by adopting Mohr-Coulomb fracture model, as shown in **Figure 5(a)**.

Thereafter, critical ductile failure points in terms of ($\bar{\varepsilon}$, η) corresponding to each type of specimens could be extracted from **Figure 5(a)**, and listed in the

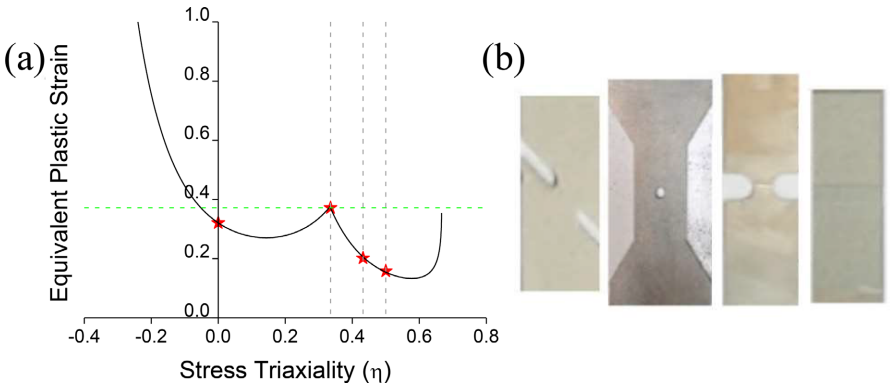

Figure 5. M-C curve of 7075-T6 Al sheet calibrated by Lee *et al.* [8], using four types of tension specimen.

Table 2, with material constants n and K values as well.

Substituting the characteristic parameters in Table 2 into Equation (11), the four variable of M-C model could be established as an analytical function through nonlinear fitting optimization. When C_1 = 0.0872, C_2 = 390 MPa, $c_\theta^s = 0.9553$ and $c_\theta^c = 1$, the overall variance of the function reaches the minimum. So far, the M-C curve for ductile fracture evaluation of 7075-T6 aluminum can be acquired as shown in Figure 6, which is completely consistent with Figure 5(a).

4.2. Measurement of M-C Curve for 1800UHSS

Three types and total nine uniaxial tension specimens (in Figure 3) from 1800UHSS sheet were loaded to fracture. Figure 7 shows the initial unloaded random-patterned images for DIC analysis. In the meanwhile the last images adjacent to the fracture for each type of specimen were also shown，illustrating the maximum deformation areas. These specimen were loaded in the Y-direction, defined as major strain ε_1, while the vertical X-direction was minor strain ε_2. Identically same as reported by Andrade *et al.* [2], for 0˚pure shear and regular tension specimens, the ductile failure initiated from the central zone of the effective deformation area, see Figure 7(a) and Figure 7(c). Whereas, the ductile failure seemed to start from the corner of the effective deformation area with respective to 45˚ shear-tension specimen, shown in Figure 7(b). In the current work,

Table 2. Parameters of critical ductile failure from four samples of 7075-T6 Al sheet.

Sample type	η	$\bar{\theta}$	$\bar{\varepsilon}_f$
Pure shear	0	0	0.321
Center hole tension	0.335	0.994	0.372
Notched tension	0.432	0.654	0.202
Plane strain tension	0.500	0.380	0.158
		n = 0.0947, K = 784.6 MPa	

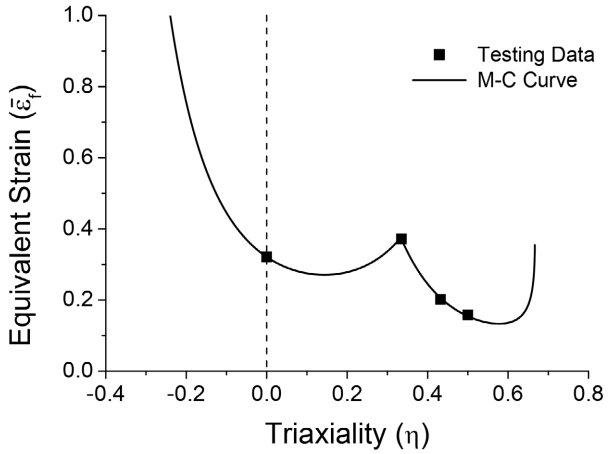

Figure 6. Calculated M-C curve of 7075-T6 Al sheet for estimating the ultimate ductile fracture.

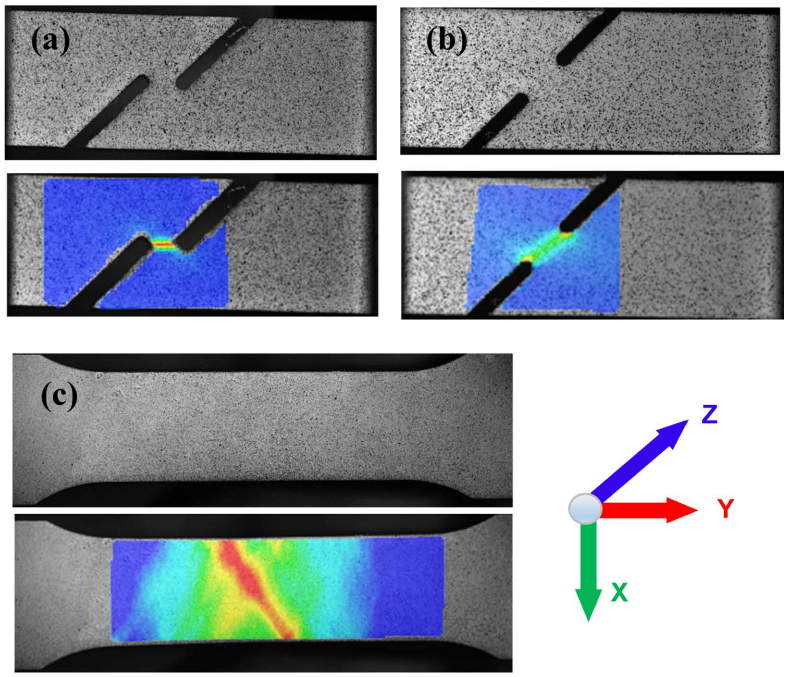

Figure 7. Illustration of three type specimens in the present study, with the initial image after random pattern preparation and the major strain distribution on the area of deformation at the critical moment of failure ((a) 0˚ pure shear; (b) 45˚ shear-tension; (c) regular tension).

wherever the ductile fracture initiated before and occurred later, the local DIC strain analysis was used to record the changes of major and minor strains confined in the fracture zone during all the testing period. In comparison with those geometrically related theoretical η values, or values calibrated by the FEM inverse identification method through force-displacement curves [2] [4], instantaneous η and $\bar{\varepsilon}_f$ of the fracture zone over the entire deformation process were experimentally determined by above Moving Regression Algorithm upon the experimental recorded (ε_1, ε_2) pairs for each specimen, which was hoped to improve the reliability of consequent M-C curve.

The critical parameters of ductile fracture relative to three types of specimens were listed in **Table 3**. Based on the same principle as mentioned above, the four variables of M-C model for 1800UHSS were obtained as C_1 = 0.12, C_2 = 1240 MPa, $c_\theta^s = 0.92$, $c_\theta^c = 1$, with respect to the determined M-C curve shown in **Figure 8**.

Figure 8 also shows the same phenomenon as reported in references [2] [3] [4]. Although geometrical-controlled uniaxial loading specimens have their stable theoretical stress triaxiality, *i.e.* η = 0 for 0˚ pure shear, η = 0.2 for 45˚ shear-tension and η = 1/3 for regular tension. Nevertheless, η was changing drastically especially at the initial loading period, due to the influence of alignment and/or the local complex deformation. Thereafter each type of specimen experienced a stable period up to end, close to their theoretical triaxiality value respectively.

At the same time, the Mohr-Coulomb model itself has the characteristic

Table 3. Parameters of critical ductile failure from three types total nine specimens of 1800UHSS sheet.

Sample type	η	$\bar{\theta}$	$\bar{\varepsilon}_f$
0˚ pure shear	0.06/0.04/0.03	0.172/0.115/0.086	0.186/0.189/0.190
45˚ tension shear	0.174/0.156/0.137	0.504/0.451/0.395	0.147/0.149/0.150
Regular tension	0.375/0.363/0.362	0.859/0.900/0.904	0.114/0.114/0.114
		$n = 0.112$, $K = 2772$ MPa	

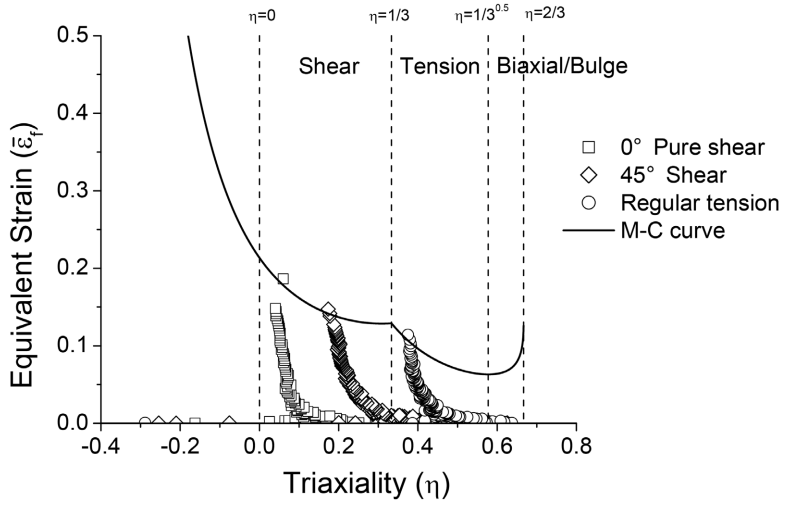

Figure 8. Calculated M-C curve of 1800UHSS sheet and the triaxiality evolution (η) of the fracture zone over the loading period relative to three types of specimens.

W-shaped in the plane stress region, *i.e.* $\eta \in (-1/3, 2/3)$. Double minimum values of $\bar{\varepsilon}_f$ occur in the shear region $\eta \in (0, 1/3)$ and the uniaxial/biaxial tension region $\eta \in (1/3, 2/3)$ (*i.e.* FLD test condition) respectively. Huang *et al.* [13] studied the ultimate ductile fracture of 1.6mm USIBOR1500 hot stamping steel sheet by choosing five types of FLD test specimens. Due to the lack of effective η values in the shearing region, the consequent M-C curve was distorted from the characteristic W-shaped into V-shaped, which maybe lead to a fail when dealing with the ductile fracture under the pure shear or shear-tension conditions.

As an effective extension of conventional FLD test (FLC) into the field of shear loading conditions, the M-C curve indicates the material ultimate resistance to the ductile fracture under common plane stress conditions, including shear, shear-tension, uniaxial tension, plane strain tension, biaxial bulging. The area under the M-C curve implies the safety margin relative to a given circumstance of triaxiality. Depending on shapes and relative positions of M-C curve obtained from different materials, it provides a practical guide to the material comparison. In **Figure 9**, M-C curves of 7075-T6 aluminum and 1800UHSS steel sheets were plotted together. It is obviously shown that 1800UHSS is completely located below that of Al sheet, which reveals that the cold working capability of

1800UHSS is so weaker at room temperature for this kind of boron-containing steel, similar to the USIBOR1500 hot stamping steel sheets as reported by Huang *et al.* [13] while their forming performance could be greatly improved by hot stamping techniques.

As to clearly compare with the conventional FLC diagram, the determined M-C model consisting of (η, $\bar{\varepsilon}$) points in implicit spherical coordinate could be inversely converted into the M-C curve, composed by the points (ε_1, ε_2) in real Cartesian-coordinate strain space, as shown in **Figure 10** and detailed in the previous work [14]. This unique type of M-C curve not only reveals the potential of material resistance performance against ductile fracture, avoiding the influence of mechanical friction caused by the regular forming test machine, but also it depicts the material property in the shearing region as well, extending the application of present FLC, same as reported by [15].

To note that when using different DIC grid sizes, such as 0.5 mm and 1 mm etc., different results of equivalent strain will be acquired. Because the smaller grid size/gauge will cause the higher strain value after DIC analysis. Therefore,

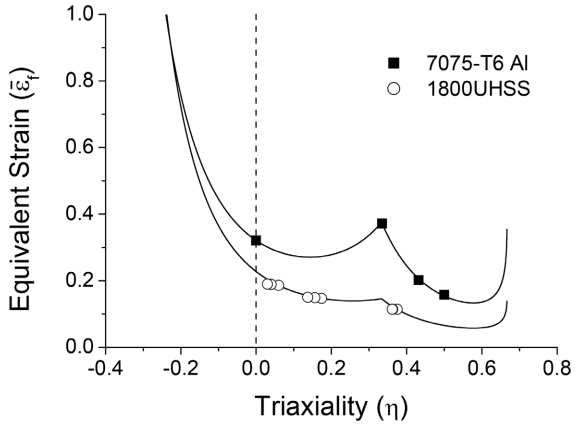

Figure 9. Comparison of the arrest performance to the ductile fracture under plane stress states, through their calculated M-C curves of 7075-T6 Al and 1800UHSS sheets.

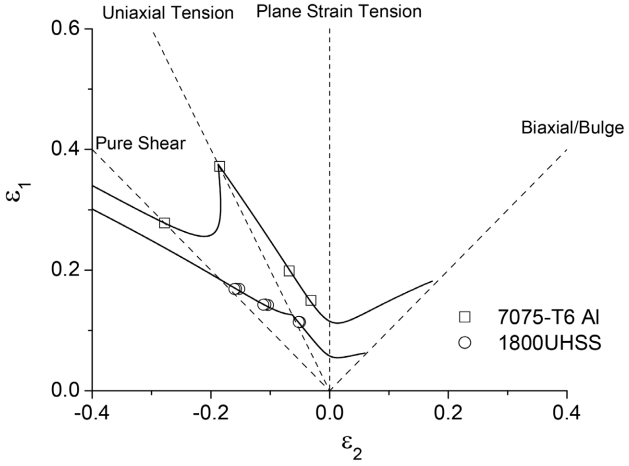

Figure 10. M-C curves compose of (ε_1, ε_2) points in real strain Cartesian-coordinate, as extended FLC curves for 7075-T6 Al and 1800UHSS sheets.

without performing regularization for results upon different initial grid size, the measured M-C curves of different materials cannot be simply compared.

Moreover, if the material local deformation could be tracked by DIC system during uniaxial loading under medium or high temperature conditions then M-C curve at high temperature can be obtained simply from same three types of specimens as mentioned above, providing a guide to study the performance evolution, caused by the temperature, which is practical to those magnesium alloy sheets and hot stamping steels as well.

5. Conclusions

The four variables Mohr-Coulomb models were introduced to study the ductile fracture of metal sheets under plane stress states. Initiating from the DIC recorded minor and major strains (ε_1, ε_2) which were distributed on the deformation area of uniaxial tension samples, several key parameters involved in the M-C model, including stress triaxiality η, Lode angle parameter $\bar{\theta}$ and equivalent strain $\bar{\varepsilon}$ over the whole loading period could be determined by Moving Regression algorithm without the involvement of FEM into industrial application. Thereafter M-C model could be solely determined through three to four well-designed specimens which have quite different theoretical stress triaxiality.

It was shown that real-tested η values changed significantly during the loading period, deviating from their theoretical values relative to the geometry. Shear loading samples are of great importance to determine M-C Curve. In the present study, three types of samples including 0˚ pure shear, 45˚ shear-tension and regular tension were testified suitable to resolve the W-shaped M-C model, which has two apparent valleys in the shear zone $\eta \in (0,1/3)$ and the uniaxial/biaxial tension zone $\eta \in (1/3, 2/3)$ respectively.

M-C curve with transformed extended-FLC curve covers shear, uniaxial tension, plane strain tension, biaxial tension/bulging loading states, effectively extending the conventional FLC into the field of shear loading, providing a guide to assess the material resistance against the ductile failures under various plane stress loading conditions.

Acknowledgements

The authors are grateful for the financial support received from the Scientific and Technical Funds provided by Central Research Institute, Baoshan Iron & Steel Co., Ltd. (Project Item Y20ECEE22F).

Conflicts of Interest

The authors declare no conflicts of interest regarding the publication of this paper.

References

[1] Bai, Y.L. and Wierzbicki, T. (2008) Forming Severity Concept for Predicting Sheet

Necking under Complex Loading Histories. *International Journal of Mechanical Sciences*, **50**, 1012-1022. https://doi.org/10.1016/j.ijmecsci.2008.02.010

[2] Andrade, F.X.C., Feucht, M., Haufe, A. and Neukamm, F. (2016) An Incremental Stress State Dependent Damage Model for Ductile Failure Prediction. *International Journal of Fracture*, **200**, 127-150. https://doi.org/10.1007/s10704-016-0081-2

[3] Park, N., Huh, H., Lim, S.J. and Seo, M.H. (2017) Fracture-Based Forming Limit Criteria for Anisotropic Materials in Sheet Metal Forming. *International Journal of Plasticity*, **96**, 1-35. https://doi.org/10.1016/j.ijplas.2016.04.014

[4] Effelsberg, J., Haufe, A., Feucht, M. and Bois, P.D. (2012) On Parameter Identification for the GISSMO Damage Model. 12*th International LS-DYNA Conference*, Detroit, USA, 1 June 2012, Metal Forming 25-a. https://www.dynalook.com/conferences/12th-international-ls-dyna-conference/metalforming25-a.pdf/view

[5] Behrens, B.-A., Bouguecha, A., Vucetic, M. and Peshekhodov, I. (2012) Characterisation of the Quasi-Static Flow and Fracture Behaviour of Dual-Phase steel Sheets in a Wide Range of Plane Stress States. *Archives of Civil & Mechanical Engineering*, **12**, 397-406. https://doi.org/10.1016/j.acme.2012.06.017

[6] Giglio, M., Manes, A., and Viganò, F. (2012) Ductile Fracture Locus of Ti-6Al-4V Titanium Alloy. *International Journal of Mechanical Sciences*, **54**, 121-135. https://doi.org/10.1016/j.ijmecsci.2011.10.003

[7] Bai, Y.L. and Wierzbicki, T. (2010) Application of Extended Mohr–Coulomb Criterion to Ductile Fracture. *International Journal of Fracture*, **161**, 1-20. https://doi.org/10.1007/s10704-009-9422-8

[8] Lee, S.K., Lee, J.S., Song, J.H. and Kim, G.H. (2018) Fracture Simulation of Cold Roll Forming Process for Aluminum 7075-T6 Automotive Bumper Beam Using GISSMO Damage Model. *Procedia Manufacturing*, **15**, 751-758. https://doi.org/10.1016/j.promfg.2018.07.314

[9] Chen, X.M., Chen, G.F., Huang, L. and Shi, M.F. (2018) Calibration of GISSMO Model for Fracture Prediction of a Super High Formable Advanced High Strength Steel. 15*th International LS-DYNA Conference*, Detroit, USA, 10 June 2018, Metal Forming 099. https://www.dynalook.com/conferences/15th-international-ls-dyna-conference/metal-forming/calibration-of-gissmo-model-for-fracture-prediction-of-a-super-high-formable-advanced-high-strength-steel/view

[10] Granum, H., Morin, D., Børvik, T. and Hopperstad, O.S. (2021) Calibration of the Modified Mohr-Coulomb Fracture Model by Use of Localization Analyses for Three Tempers of an AA6016 Aluminium Alloy. *International Journal of Mechanical Sciences*, **192**, Article ID: 106122. https://doi.org/10.1016/j.ijmecsci.2020.106122

[11] Andrade, F., Feucht, M. and Haufe, A. (2014) On the Prediction of Material Failure in LS-DYNA®: A Comparison between GISSMO and DIEM. 13*th International LS-DYNA Conference*, Detroit, USA, 1 June 2014, Constitutive Modeling 123. https://www.dynalook.com/conferences/13th-international-ls-dyna-conference/constitutive-modeling/on-the-prediction-of-material-failure-in-ls-dyna-r-a-comparison-between-gissmo-and-diem/view

[12] Andrade, F. and Feucht, M. (2017) A Comparison of Damage and Failure Models for the Failure Prediction of Dual-Phase Steels. 11*th European LS-DYNA Conference*, Salzburg, Austria, 5 May 2017, 03. https://www.dynalook.com/conferences/11th-european-ls-dyna-conference/crash-metal-failure/a-comparison-of-damage-and-failure-models-for-the-failure-predicti

on-of-dual-phase-steels/view

[13] Huang, G., Zhu, H., Sriram, S., and Faruque, O. (2014) Fracture Prediction and Correlation of AlSi Hot Stamped Steels with Different Models in LS-DYNA®. 13*th International LS-DYNA Conference*, Detroit, USA, 1 June 2014, Automotive 052. https://www.dynalook.com/conferences/13th-international-ls-dyna-conference/automotive/fracture-prediction-and-correlation-of-alsi-hot-stamped-steels-with-different-models-in-ls-dyna-r/view

[14] Fang, J. and Zhang, J.W. (2020) Comments on "Ductile Fracture Prediction for Metal Sheets Using All-Strain-Based Anisotropic eMMC Model, International Journal of Mechanical Sciences 115-116 (2016) 516-531, by Y. Jia, Y. Bai". *International Journal of Mechanical Sciences*, **171**, Article ID: 105376. https://doi.org/10.1016/j.ijmecsci.2019.105376

[15] Li, Y., Luo, M., Gerlach, J. and Wierzbicki, T. (2010) Prediction of Shear-Induced Fracture in Sheet Metal Forming. *Journal of Materials Processing Technology*, **210**, 1858-1869. https://doi.org/10.1016/j.jmatprotec.2010.06.021s